

A numerical model for coarsening in wet foams with a realistic bubble-scale structure

1. Introduction

- **Coarsening** is caused by gas diffusion through the liquid in a foam, and results in the growth of large bubbles while small ones shrink [1].
- This process is not well understood in **wet foams**, where applications include fire suppression [2]. What are the growth rates of individual bubbles at moderate liquid fractions ϕ , where Plateau's laws are not satisfied, and how does the foam's macroscopic evolution change with ϕ ?
- Experiments are challenging due to drainage [3], and simulations [4, 5] have not yet fully reproduced existing experimental results.
- We present a novel numerical model for coarsening in **two-dimensional** wet foams, which allows accurate bubble deformation and gas diffusion through films and Plateau borders, and which implements a qualitatively-realistic **disjoining pressure**.
- We exhibit results obtained by applying this model to coarsening in a **defective hexagonal foam**, where we investigate a transition in behaviour between larger and smaller ϕ .

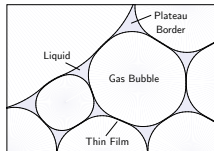


Figure 1: The structure of a two-dimensional wet foam.

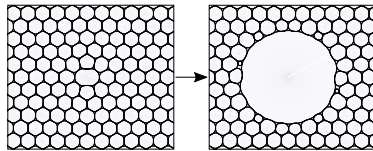


Figure 2: Simulated coarsening of a defective hexagonal foam with liquid fraction $\phi = 0.056$.

2. Structural model of the foam

- Using a **finite-element** approach, the liquid/gas interfaces are **vertices** joined by straight **edges**. Bubble rearrangements occur naturally as there is no intrinsic difference between the thin films and Plateau borders.
- The foam's total interface energy is [1]

$$E = \int_{\Gamma} \gamma(\mathbf{r}) dl; \quad (1)$$

where Γ represents all liquid/gas interfaces. The surface tension γ varies with position \mathbf{r} due to the **disjoining pressure**, stopping overlaps.

- We equilibrate the foam by using **conjugate gradient** iterations to minimise E , subject to fixed bubble areas. Hence, our approach is **quasi-static**, suitable for the slow [6] process of coarsening.
- Our approach adapts that of ref. [7], and is similar to that of ref. [8]. To our knowledge, this approach has not yet been applied to coarsening.
- We implement our simulations in the **Surface Evolver** [9].

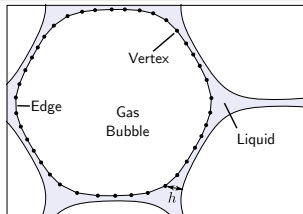


Figure 3: The discretisation in our structural model, including the local film thickness h .

3. Disjoining pressure

- We use a qualitatively-realistic DLVO [10] **disjoining pressure**

$$\Pi(h) = A(1 - \alpha h)e^{-h/h_0}, \quad (2)$$

where h is the **film thickness**. The parameters are set to obtain an **equilibrium film thickness** h_0 and film-border **contact angle** θ (Figure 4). Although we set $\theta = 0$, Π is still attractive at larger h .

- The surface tension depends upon Π via [10]

$$\gamma(h) = \gamma_{\infty} + \frac{1}{2} \int_h^{\infty} \Pi(s) ds, \quad (3)$$

where γ_{∞} is the surface tension of an isolated interface.

- The interfaces are curved in general, so we take h to be the shortest distance to a neighbouring interface (Figure 3). Similarly to ref. [11], we ignore film curvature in equations (2–3) as an approximation.

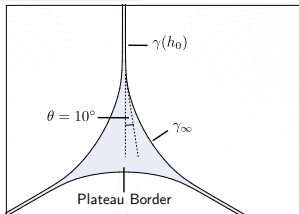


Figure 4: The film-border contact angle θ [11]. Our results use $\theta = 0$.

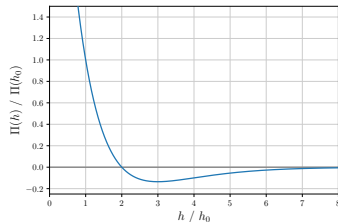


Figure 5: Our model disjoining pressure for $\theta = 0$.

4. Validation of the structural model

- We validate our structural model using the rheology of a **sheared hexagonal foam** (Figure 6) [12, 13], since this is independent of our coarsening implementation.
- We apply a **simple shear** to a periodic domain containing one bubble with effective radius R , measuring the **shear stress** τ_{yx} at each **strain** ϵ .
- Our stress-strain curves (necessarily for film thickness $h_0 > 0$) are compared with ref. [12] (for $h_0 = 0$) in Figure 7, using that the bubble deformation is the same for any h_0 at a fixed **effective liquid fraction** ϕ_{eff} [12]. We observe good agreement, which improves for smaller h_0 . The additional peaks in our curves are due to the disjoining pressure's attractive component.
- We plot our foam's **shear modulus** G , fitted using the analytic stress-strain relation [13], in Figure 8 alongside the analytic result [13]

$$G = \sqrt{\frac{1 - \phi}{2\pi}} \frac{3^{1/4} \gamma_{\infty}}{R}. \quad (4)$$

Close agreement is observed, except near to the **jamming transition** $\phi \approx 0.09$ [1] — possibly because ref. [13] assume that interfaces are either parts of films or Plateau borders, with no **transition region** [1].

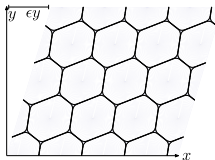


Figure 6: A finite portion of a simply-sheared hexagonal foam, at strain ϵ and with liquid fraction $\phi = 0.02$. We let $\epsilon = 0$ correspond to a symmetric state.

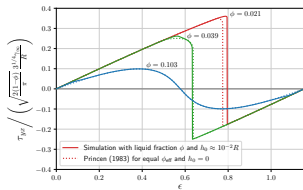


Figure 7: Comparison of simulated stress-strain curves with ref. [12], using 384 vertices.

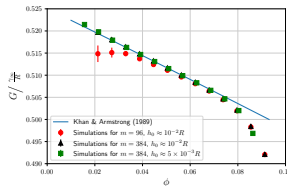


Figure 8: Comparison of our simulated shear modulus with ref. [13], for several liquid fractions ϕ , film thicknesses h_0 , and numbers of vertices m . The error bars relate to the fit of G .

5a. Coarsening

- The concentration c of gas dissolved in a foam's liquid is given by **Laplace's equation** $\nabla^2 c = 0$, with $c = Hp$ on the interfaces; p is the bubble pressure, and H is Henry's constant [1, 14]. The gas concentration gradients result in its diffusion, and thus coarsening [14].
- Following ref. [14], we approximate the gas flow rate per unit length f , between adjacent bubbles through an element of interface, by [1]

$$f = \frac{\kappa H \Delta p}{h}; \quad (5)$$

where κ is a constant, Δp is the pressure difference between the bubbles, and h is the local film thickness. This is exact for infinite parallel planar interfaces.

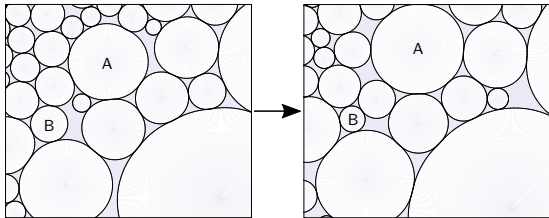


Figure 9: A disordered foam with liquid fraction $\phi = 0.103$ before and after a period of coarsening. A is a large bubble that has grown, and B is a small bubble that has shrunk.

5b. Defective hexagonal foam

- We use a **defective hexagonal foam** as a model system for coarsening. These have been studied numerically in the dry limit [15], and at liquid fraction $\phi = 0.05$ [16]. We are not aware of any systematic investigations over a range of ϕ .
- The system is obtained by bursting one film in a monodisperse hexagonal foam (Figure 10) [17]. This is termed a Type I defect [16].
- No coarsening occurs in a monodisperse hexagonal foam [6]. However, in the dry limit, a Type I defect grows under coarsening without bound, becoming circular, with a linearly increasing radius [15, 17].
- At $\phi = 0.05$ considered by ref. [16], a **disordered region** instead emerges around the initially defective bubble, which grows faster than the latter and contains additional large bubbles.

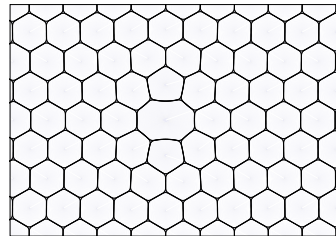


Figure 10: A defective hexagonal foam with liquid fraction $\phi = 0.021$. We refer to the large bubble as the **initially defective bubble**.

6. Coarsening results for the model system

- We coarsen a defective hexagonal foam at liquid fractions $\phi \in [0.021, 0.103]$, in a periodic domain with 255 bubbles. The film thickness is $h_0 \approx 10^{-2} R$, where $R = 0.909$ is the effective bubble radius in the initial hexagonal foam, for which $\phi = 0.103$ is the **jamming transition** at this h_0 [12].
- For $\phi \lesssim 0.091$, the **dry-type** coarsening behaviour of ref. [15] is observed (Figures 12–13), including the eventual linear growth of the effective radius R_d of the initially defective bubble (Figure 11). The growth rate decreases as ϕ increases, because the gas flow is reduced by larger Plateau borders [14].
- For $\phi \gtrsim 0.091$, the **wet-type** behaviour of ref. [16] emerges (Figures 14–15). Hence, we find a larger transition liquid fraction than ref. [16], which may be due to the allowed deformation of our bubbles, unlike in the Durian bubble model they use.
- It remains possible that a wet-type disordered region emerges for smaller ϕ at times beyond the end of our simulations. However, this region arises before half the stopping time at $\phi = 0.091$.
- Some dependence on the simulation convergence parameters remains for the bubble configurations in the wet-type disordered regions. However, the corresponding statistics (Section 7) are robust, as is the ϕ value at which the observed transition occurs. We have not yet investigated dependence upon h_0 .

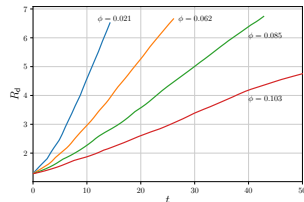


Figure 11: The effective radius of the initially defective bubble against dimensionless time, for several liquid fractions.

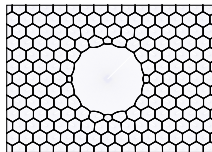


Figure 12: Foam with $\phi = 0.021$ coarsened to dimensionless time $t = 10$.

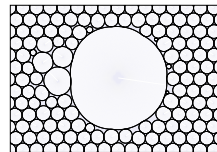


Figure 14: Foam with $\phi = 0.091$ coarsened to dimensionless time $t = 50$.

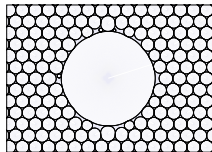


Figure 13: Foam with $\phi = 0.085$ coarsened to dimensionless time $t = 40$.

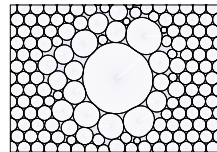


Figure 15: Foam with $\phi = 0.103$ coarsened to dimensionless time $t = 50$.

7. Statistical results in the defective region

- Similarly to ref. [18], we define the **defective region** around (and omitting) the initially defective bubble to contain all other bubbles without exactly 6 neighbours, or with a neighbour without 6 neighbours.
- In Figures 16–17, we plot the mean bubble area $\langle A \rangle$ and **geometric disorder** [1]

$$\sigma_A = \sqrt{\frac{\langle A^2 \rangle}{\langle A \rangle^2} - 1} \quad (6)$$

in the defective region, against the effective radius R_d of the initially defective bubble (for comparability between different liquid fractions ϕ).

- For $\phi \lesssim 0.091$ (the **dry-type** regime), the curves remain close for nearby ϕ . The geometric disorder appears to oscillate around a constant value, consistent with the existence of a previously-suggested scaling state in the defective region [18].
- For $\phi \gtrsim 0.091$ (the **wet-type** regime), the curves eventually separate from the dry-type curves, increasing thereafter almost monotonically at higher ϕ ; $\langle A \rangle$ is qualitatively consistent with ref. [16]. This coincides with the eventual appearance of large bubbles in the defective region.
- Hence, $\langle A \rangle$ and σ_A in the defective region are quantitative measures of the transition between dry-type and wet-type behaviour. The polydispersity behaves similarly, although patterns in μ_2 (the variance of the number of neighbours) are not as easy to discern.

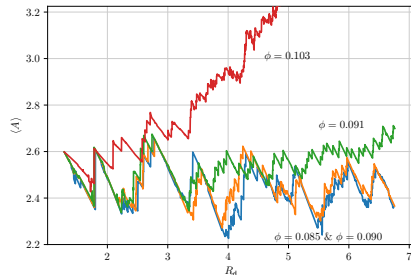


Figure 16: The mean area of bubbles in the defective region against the initially defective bubble's effective radius, for various liquid fractions.

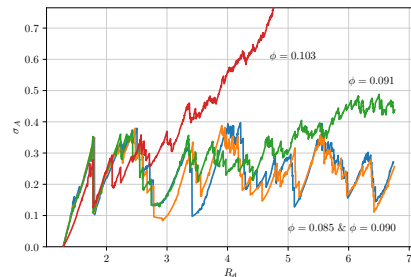


Figure 17: The geometric disorder in the defective region against the initially defective bubble's effective radius, for various liquid fractions.

8. Outlook

- We have applied our exhibited numerical coarsening model to defective hexagonal foams, giving evidence that their behavioural transition, which is quantified by features in the bubble statistics, occurs at liquid fraction $\phi \approx 0.09$.
- Our primary aim is to use our simulation approach to study coarsening in disordered wet foams, in two and three dimensions. Progress in adapting a similar structural model to three dimensions was made by ref. [19].
- Such work may contribute to answering unresolved questions regarding wet-foam coarsening, including the growth rates of individual bubbles at intermediate liquid fractions ϕ for which Plateau's laws do not hold.
- Recent experiments on the International Space Station should provide data against which our simulations may be compared [20].
- We also intend to continue investigating defective hexagonal foams, to better understand the cause and properties of the behavioural transition. This work may be relevant to disordered foams, where any behavioural transitions would likely be more challenging to identify.
- We aim to further validate our coarsening model by comparing its predictions of bubble growth rates with those obtained via accurate solutions of Laplace's equation.

Acknowledgements

Funded by ESA REFOAM MAP contract 4000129502.

References

- [1] Cantat I et al. *Foams: Structure and Dynamics*. Trans. by Flatman R. Oxford (GB): Oxford University Press, 2013. 265 pp.
- [2] Laundess AJ et al. *Fire Technol.* **47** (2011), 149–162. DOI: 10.1007/s10694-009-0136-2.
- [3] Isert N, Maret G, and Aegerter CM. *Eur. Phys. J. E* **36**(10) (2013), 116. DOI: 10.1140/epje/i2013-13116-x.
- [4] Fortuna I et al. *Phys. Rev. Lett.* **108**(24) (2012), 248301. DOI: 10.1103/PhysRevLett.108.248301.
- [5] Khakalo K et al. *Phys. Rev. E* **98**(1) (2018), 012607. DOI: 10.1103/PhysRevE.98.012607.
- [6] Weaire D and Hutzler S. *The Physics of Foams*. New York (US-NY): Oxford University Press, 1999. 246 pp.
- [7] Kähärä T, Tallinen T, and Timonen J. *Phys. Rev. E* **90**(3) (2014), 032307. DOI: 10.1103/PhysRevE.90.032307.
- [8] Boromand A et al. *Phys. Rev. Lett.* **121**(24) (2018), 248003. DOI: 10.1103/PhysRevLett.121.248003.
- [9] Brakke KA. *Exp. Math.* **1**(2) (1992), 141–165. DOI: 10.1080/10586458.1992.10504253.
- [10] Langevin D. *Emulsions, Microemulsions and Foams*. Cham (CH): Springer, 2020. 344 pp.
- [11] Denkov ND, Petsev DN, and Danov KD. *J. Colloid Interf. Sci.* **176**(1) (1995), 189–200. DOI: 10.1006/jcis.1995.0022.
- [12] Princen HM. *J. Colloid Interf. Sci.* **91**(1) (1983), 160–175. DOI: 10.1016/0021-9797(83)90323-5.
- [13] Khan SA and Armstrong RC. *J. Rheol.* **33**(6) (1989), 881–911. DOI: 10.1122/1.550068.
- [14] Schimming CD and Durian DJ. *Phys. Rev. E* **96**(3) (2017), 032805. DOI: 10.1103/PhysRevE.96.032805.
- [15] Ruskin HJ and Feng Y. *J. Phys.: Condens. Matter* **7**(43) (1995), L553–L559. DOI: 10.1088/0953-8984/7/43/001.
- [16] Gardiner BS, Dlugogorski BZ, and Jameson GJ. *J. Phys.: Condens. Matter* **11**(28) (1999), 5437–5453. DOI: 10.1088/0953-8984/11/28/305.
- [17] Chae JJ and Tabor M. *Phys. Rev. E* **55**(1) (1997), 598–610. DOI: 10.1103/PhysRevE.55.598.
- [18] Jiang Y, Mombach JCM, and Glazier JA. *Phys. Rev. E* **52**(4) (1995), R3333–R3336. DOI: 10.1103/PhysRevE.52.R3333.
- [19] Wang D et al. *Soft Matter* **17**(43) (2021), 9901–9915. DOI: 10.1039/D1SM01228B.
- [20] Born P et al. *Rev. Sci. Instrum.* **92**(12) (2021), 124503. DOI: 10.1063/5.0062946.